The 6th International Conference on Renewable Power Generation (RPG)

19–20 October 2017

Modelling and control of a VSC medium-voltage DC distribution network with DFIG wind farm

Simiyu Patrobers, Xin Ai, Bitew Girmaw Teshager, Wang Kunyu

State Key Laboratory, Alternate Electrical Power Systems with Renewable Energy Sources, North China Electric Power University, Beijing, 102206, People's Republic of China
E-mail: 1154300005@ncepu.edu.cn

Published in *The Journal of Engineering*; Received on 12th October 2017; Accepted on 2nd November 2017

Abstract: The voltage source converters (VSC) medium-voltage DC (MVDC) is the future distribution network for integrating renewable energy sources. The doubly fed induction generator (DFIG) wind turbine is the most efficient option for wind farm application. The intermittency of wind power is challenging in grid integration at the AC distribution system level. This study presents a ±10 kV VSC MVDC network with DFIG wind farm integrated to mitigate these effect. Key MVDC network components and controllers are modelled including the control strategy for the MVDC grid. The proposed system is validated in MATLAB/SIMULINK for steady state and transient conditions. The results show that the MVDC can work as firewall that absorbs the fluctuating wind power to a stable system with good power flow and balance as well as constant DC voltage. Therefore, the MVDC network is a stable system with fast dynamic response.

1 Introduction

The MVDC concept was initially explored for naval ship applications but with advances in voltage source converter (VSC) technology and rapid growth in end-user DC loads in power systems, the focus has shifted to grid applications [1–3]. MVDC unlike medium-voltage AC (MVAC) systems involves fewer energy conversion stages, which increases efficiency of the whole supply and distribution system. Hence, the MVDC system can be an enabling platform for grid integration of wind and solar photovoltaic (PV), energy storage, fuel-cell, and supply of DC loads [1, 2, 4–6].

Bathurst *et al*., in [2], summarized the benefits of MVDC, which include: better utilisation of the existing AC network assets; avoided investment in network reinforcement; reduced losses in other network equipment; applicable power converters contributing no fault current; reactive power support and voltage control due to use of four-quadrant VSC and feasibility of developing a multi-terminal DC (MTDC) grid.

Global research in MVDC distribution network has grown rapidly although there is no commercial terrestrial installation to date. At a new campus of the Aachen University in Germany, an MVDC network has been proposed and assessed for supplying high power laboratories benches [6, 7]. The US Navy proposed an MVDC distribution system dubbed the 'Next Generation Integrated Power System (NGIPS) Roadmap' naval shipboard power systems [1, 3]. In China, the Shenzhen Power Bureau at the Shenzhen Baolong City set up a national MVDC demonstration project to provide reference in research and application. On this basis, the China Southern Power Grid and several universities have set up a real-time simulation laboratory to further research in MTDC/MVDC distribution network [2, 8].

Wind power is the most economical and fastest growing renewable energy source due to developments in commercial wind turbine generator designs. The VSC-based doubly fed induction generator (DFIG) is the most popular variable speed wind turbine. It is able to extract maximum power over a wide range of wind speeds achieving maximum aerodynamic efficiency; hence, it is the main choice for wind farm applications. Besides, DFIG achieves grid code requirements such as continuous reactive power and frequency support as well as fault ride-through capability [9–11].

Studies have been undertaken on MVDC system for: electrical charging stations powered by solar PV [5], data centre distribution systems [11], deployment of wind power [12, 13] amongst others. MVDC control, protection, and operation issues have been investigated but remain challenging and research is still ongoing. As a major part of the future commercial distribution system, the challenges need to be addressed to attain these MVDC futuristic visions [13, 14].

In this context, the stochastic nature of wind remains a challenge especially in the AC distribution network. When the wind power is integrated, poor voltage regulation, feeder over-loading and reverse power flow occur [13, 15]. MVDC network can improve the distribution network efficiency and quality of supply [2, 15]. This paper investigates a VSC MVDC network as a platform of transforming the intermittent DFIG wind farm energy to a controllable and predictable supply. It is organised as follows: modelling of VSC MVDC network is presented in Section 2. Simulation results of the network are presented in Section. 3. Finally, the conclusion is drawn in Section 4.

2 VSC MVDC network

2.1 DFIG wind turbine model

The MVDC system for the study in Fig. 1 comprises the DFIG wind farm, the wind farm side VSC connected to the AC grid side VSC through an MVDC link and the DC load. The DFIG consists of a wound rotor induction generator with stator windings connected directly to the AC grid. The rotor windings are connected to the grid through a variable frequency AC/DC/AC VSC namely the rotor-side converter (RSC) and grid-side converter (GSC). The induction generator is connected to the wind turbine by means of a gear-box system. A crowbar is provided at the rotor windings for over-current protection.

The aerodynamic model of the wind turbine is described by C_p–λ–β characteristics. The power coefficient (C_p) is a function of pitch

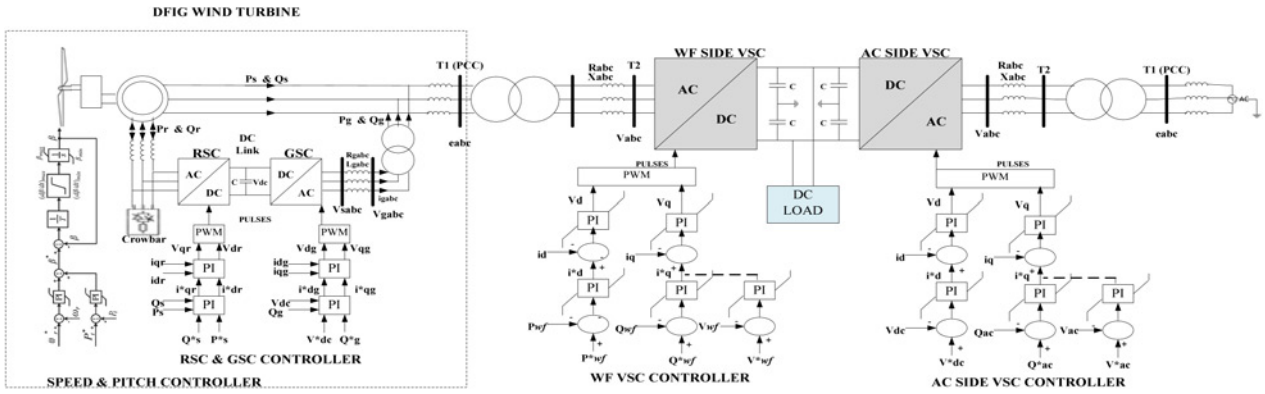

Fig. 1 *VSC MVDC network*

angle (β) and tip speed ratio (λ) that shows the overall efficiency of the wind turbine. Given C_p of a wind turbine rotor, the total mechanical power (P_t) extracted from wind is given by [9]

$$P_t = \frac{1}{2}\rho A C_p(\lambda, \beta)V^3, \tag{1}$$

where $\lambda = W_t R/V$ and ρ is the air density, A is the area covered by the rotor, V is the wind velocity, λ is the ratio of the blade tip speed to the wind speed upstream the wind turbine rotor, W_t is the rotor speed and R is the length of the blade.

At a given wind speed, there is a specific wind turbine speed that attains maximum C_p extracting maximum wind power. When the wind speed is below the rated value, the wind turbine operates in variable-speed mode regulated by the active power control shown in Fig. 1. Maximum C_p is realised, pitch control is deactivated and β is fixed. However, if the wind speed is above the rated value, the wind turbine speed (W_r) is regulated by the pitch control, which increases the pitch angle reducing the total power extracted from the wind [10, 14].

The RSC independently regulates the DFIG stator active power (P_s) and stator reactive power (Q_s). The reference and the measured signals of P_s and Q_s are compared and the error signals obtained then passed through the proportional integral (PI) controllers to give i_{qr}* and i_{dr}* reference current signals as shown in Fig. 1. These are further compared to the corresponding measured current signals to form two voltage signals. The voltage signals are compensated by the corresponding dq cross-coupling voltages to form V_{qr} and V_{dr} signals that are then channelled to the pulse-width modulation (PWM) to give pulse signals for RSC control [10, 16].

The GSC controls the DC link voltage and the reactive power exchange between the AC grid and the GSC as shown in Fig. 1. It generates i_{dg}* and i_{qg}* reference signals, which are compared to the corresponding measured signals to give two voltage signals. The voltage signals are compensated by the corresponding dq cross coupling voltages to form V_{qg} and V_{dg}, which are ultimately channelled to the PWM to derive pulse signals for the GSC control [10, 14, 16].

2.2 Wind-farm side VSC model

In the wind farm side VSC, the outer controllers are modelled considering the apparent power S_{wf} at the point of common coupling (PCC) [17] in Fig. 1. The wind farm side VSC model in dq frame is given as

$$\begin{aligned} S_{wf} &= \frac{3}{2}e_{dq}i_{dq}^{*} = \frac{3}{2}\left(e_d + je_q\right)\left(i_d - ji_q\right), \\ S_{wf} &= \frac{3}{2}\left\{\left(e_d i_d + e_q i_q\right) + j\left(e_q i_d - e_d i_q\right)\right\}. \end{aligned} \tag{2}$$

Aligning the AC voltage vector e_d with the d-axis results in $e_q = 0$. The wind farm active and reactive power is given as

$$\begin{aligned} P_{wf} &= \frac{3}{2}e_d i_d \rightarrow i_d^{*} = \frac{2P^{*}}{3e_d}, \\ Q_{wf} &= -\frac{3}{2}e_d i_q \rightarrow i_q^{*} = \frac{2Q^{*}}{3e_d}. \end{aligned} \tag{3}$$

At the PCC, the AC voltage is given in (4). The input current vector i_s equals (5)

$$\hat{e} - \hat{v} = (R + j\omega L)\hat{i}_s, \tag{4}$$

$$\hat{i}_s = \left(\frac{S_{wf}}{e}\right)^{*} = \left(\frac{P_{wf} + jQ_{wf}}{e}\right)^{*} = \left(\frac{P_{wf} - jQ_{wf}}{e}\right). \tag{5}$$

The voltage at the PCC is given as (6). Taking the real parts gives (7); hence, AC voltage is controlled by reactive power

$$\begin{aligned} \hat{e} &= \hat{v} + (R + j\omega L)\left(\frac{P_{wf} - jQ_{wf}}{e}\right) \\ &\hat{v} + \left(\frac{P_{wf}r + \omega L Q_{wf}}{e}\right) + j\left(\frac{P_{wf}\omega L - Q_{wf}r}{e}\right), \end{aligned} \tag{6}$$

$$\begin{aligned} \hat{e} &= \hat{v} + \left(\frac{P_{wf}r + \omega L Q_{wf}}{e}\right), \\ \Delta e &= \frac{\omega L}{e}\Delta Q_{wf}. \end{aligned} \tag{7}$$

For inner controllers, (8) is derived at the PCC. The three-phase currents and voltages are then transformed to dq [17, 18]

$$\begin{aligned} e_{abc} - v_{abc} &= Ri_{abc} + L\frac{d}{dt}i_{abc}, \\ L\frac{d}{dt}i_{dq} &= e_{dq} - v_{dq} - Ri_{dq} \pm j\omega L. \end{aligned} \tag{8}$$

Taking the Laplace transform, the input phase current is given in (9). The d and q axes are cross coupled due to the cross terms ωLi_q and ωLi_d but are compensated by feed-forward for independent control of the dq-axes components

$$\begin{aligned} sLi_d &= e_d - v_d - Ri_d + j\omega Li_q, \\ sLi_q &= e_q - v_q - Ri_q - j\omega Li_d. \end{aligned} \tag{9}$$

The active current, (i_d) controls the wind farm active power to the DC-link while the reactive current (i_q) controls reactive power

exchanged between the wind farm side VSC and the DFIG as well as the AC voltage as shown in Fig. 1. In principle, the reactive power reference can be set to zero. The reactive power exchanged controls the wind farm AC voltage. The measured and reference signals for the active power and AC voltage are compared to give the error signals which are passed to the PI controllers to generate i_{dr}* and i_{qr}* reference signals. These are compared with the measured wind farm currents to give error signals for generating voltage signals in the inner controller. The voltage signals are passed to the PI controllers which are then compensated by feed forward voltage terms and connected to PWM for giving pulses for the wind farm side VSC control [10, 17, 18, 21].

2.3 AC grid side VSC model

The power balance between the AC system and the MVDC is given in (10) [17] (Fig. 1). The current through the DC link capacitor (i_c) is expressed in (11) and the DC voltage is in (12)

$$\begin{aligned} P_{ac} - P_{dc} - P_c - P_{loss} &= 0, \\ \frac{3}{2} e_d i_d - P_{dc} - V_{dc} i_c - P_{loss} &= 0, \end{aligned} \tag{10}$$

$$i_c = C\frac{dV_{dc}}{dt} = \left\{\frac{3e_d i_d}{2V_{dc}} - \frac{P_{dc} + P_{loss}}{V_{dc}}\right\}, \tag{11}$$

$$\frac{dV_{dc}}{dt} = \frac{1}{C}\left(\frac{3e_d i_d}{2V_{dc}} - \frac{P_{dc} + P_{loss}}{V_{dc}}\right) = \frac{3e_d}{2V_{dc}C}\left(i_d - \frac{2P_L}{3V_{dc}}\right), \tag{12}$$

where P_{ac}, P_{dc}, P_c and P_{loss} are active power in the AC network and DC link, DC link capacitor active power and converter power losses, respectively. The reactive power exchanged between the AC system and the AC side VSC as well as the AC voltage and the inner controllers are similarly and correspondingly derived like in the wind farm side VSC model. Additionally, the procedure similar to the wind farm side VSC model is then followed to get relevant reference signals for generating pulses for AC grid side VSC control. Hence, the active current controls the DC link voltage which regulates the active power balance between the DC grid and AC system. The reactive current controls AC grid voltage by regulating the reactive power exchanged between the AC grid side VSC and the AC system [10, 17, 18, 21] as shown in Fig. 1.

2.4 MVDC-link model

A lumped parameter cable model with identical π-sections has a numerically stable transient behaviour than other distributed cable models [19] hence used in the study. Fig. 2 shows a DC π-cable model with converters; C_{c1} and C_{c2}.

The dynamics of the voltages and currents in the DC cable are given as (13) and (14), respectively, where C_{eq} is the equivalent DC capacitor [19]

$$\begin{aligned} \frac{dV_{dc1}}{dt} &= \frac{1}{C_{eq}}(i_1 - i_{cc}), \\ \frac{dV_{dc2}}{dt} &= \frac{1}{C_{eq}}(i_2 + i_{cc}), \end{aligned} \tag{13}$$

$$\frac{di_{cc}}{dt} = \frac{1}{L}(V_{dc1} - Ri - V_{dc2}). \tag{14}$$

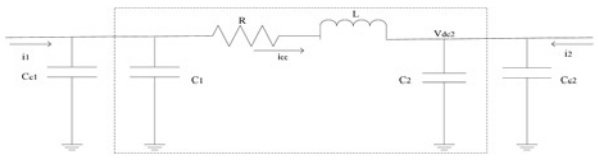

Fig. 2 *DC π-cable model [19]*

2.5 AC grid side model

The primary, secondary transformer voltages and converter voltages are given as e_{t1}, e_{t2}, and V, respectively, in Fig. 1. The phase voltage relations across the reactor and the transformer are given in (15) and (16), where X and X_L are their reactances [20]. dq transformation of (15) gives (17). Similar transformation of (16) gives (18) and (19)

$$[e_{t2abc} - V_{abc}] = \left\{\frac{X}{\omega}\frac{d(i_{abc})}{dt} + Ri_{abc}\right\}, \tag{15}$$

$$[e_{t1abc} - e_{t2abc}] = \frac{X_L}{\omega}\frac{d(i_{abc})}{dt}, \tag{16}$$

$$\left\{\frac{X}{\omega}\frac{d(i_{dq})}{dt} \mp Xi_{qd}\right\} = [e_{t2dq} - Ri_{dq} - V_{dq}], \tag{17}$$

$$[e_{t2d} - e_{t1d}] = X_L i_q - \frac{X_L}{\omega}\frac{d(i_d)}{dt}, \tag{18}$$

$$[e_{t1q} - e_{t2q}] = X_L i_d - \frac{X_L}{\omega}\frac{d(i_q)}{dt}. \tag{19}$$

We neglect the current dynamics in the transformer in (18) and (19). Aligning the q-axis of the dq frame with the AC system voltage e_{t1}, let $e_{t1d}=0$ hence (20) and (21) hold

$$e_{t2d} = X_L i_q, \tag{20}$$

$$[e_{t1q} - e_{t2q}] = X_L i_d. \tag{21}$$

Add (18) and (19), respectively, to (20) and (21) to form AC side model as

$$\left\{\frac{X}{\omega}\frac{d(i_d)}{dt} - (X + X_L)i_q\right\} = [-Ri_d - V_d], \tag{22}$$

$$\left\{\frac{X}{\omega}\frac{d(i_q)}{dt} + (X + X_L)i_d\right\} = [e_{t1q} - Ri_q - V_q]. \tag{23}$$

3 Simulation results

The proposed VSC MVDC network with DFIG wind farm performance is evaluated through MATLAB/SIMULINK simulation. The DFIG wind farm and an ideal AC grid supplies power to the MVDC bus as shown in Fig. 1. Important parameters for the MVDC network are shown in Appendix 1.

The constant DC voltage control; constant active power control, constant AC voltage and frequency conversion control are the possible control schemes for a VSC on the DFIG and the AC grid sides. However, this paper uses the constant active power control (DFIG Wind farm VSC side) and constant DC voltage control (AC grid

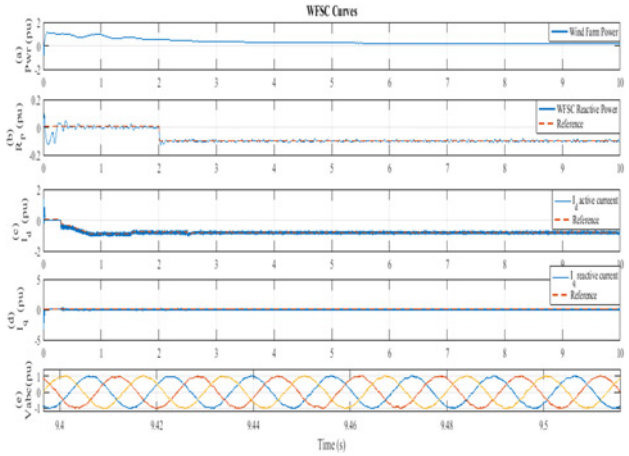

Fig. 3 *WFSC curves for steady-state operation*

side). The network dynamic behaviour is evaluated under variable wind speeds in steady state and transient state conditions.

3.1 Steady-state operation

The DFIG wind speeds are varied from 15 m/s to below the wind turbine minimum speed and the results are as shown in Figs. 3 and 4. When the wind speed falls, the corresponding power output falls as expected in Fig. 3*a*. The dropping wind active power flow allows more power from the AC grid as shown in Fig. 4*f* to sustain the active power balance with the MVDC which provides a stable supply for efficient operation of the DC motor load through the DC/DC converters.

The active current, (i_d) in Fig. 3*c* accurately controls the varying wind farm side VSC active power to the MVDC link. On the other hand, the active current component on the AC grid side in Fig. 4*c* controls the DC link voltage shown in Fig. 4*a* that manages the active power balance between the MVDC grid/load and the DFIG wind farm and AC system.

It is also be observed that the reactive power at the wind farm VSC side and the AC grid VSC side are accurately and independently controlled as shown in Figs. 3*b* and 4*b*, respectively. This is shown in the way the reactive current (i_q) in Figs. 3*d* and 4*d* accurately traces their respective reference values without any deviations. The efficient reactive power exchange capability support the stability of AC voltage as shown in Figs. 3*e* and 4*e* at the DFIG wind farm and the AC grid, respectively.

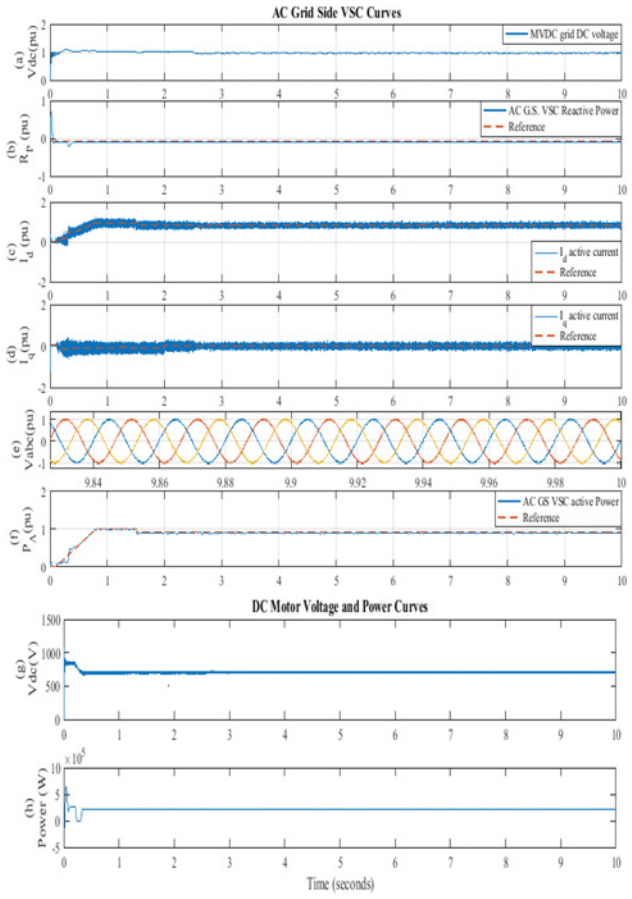

Fig. 4 *AC grid side VSC for steady-state operation*

3.2 Transient operation

When a three-phase fault is imposed on the DFIG wind farm VSC and AC grid VSC sides at $t = 3.0–3.05$ s and $t = 7.0–7.05$ s, respectively, the system response is shown in Figs. 5 and 6. On the wind

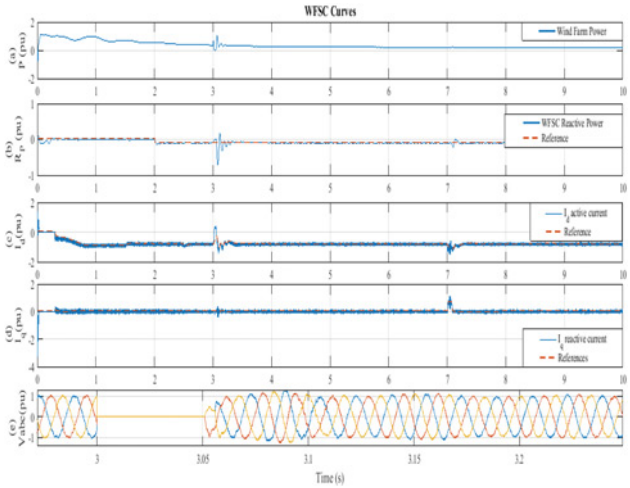

Fig. 5 *WFSC curves for three-phase fault*

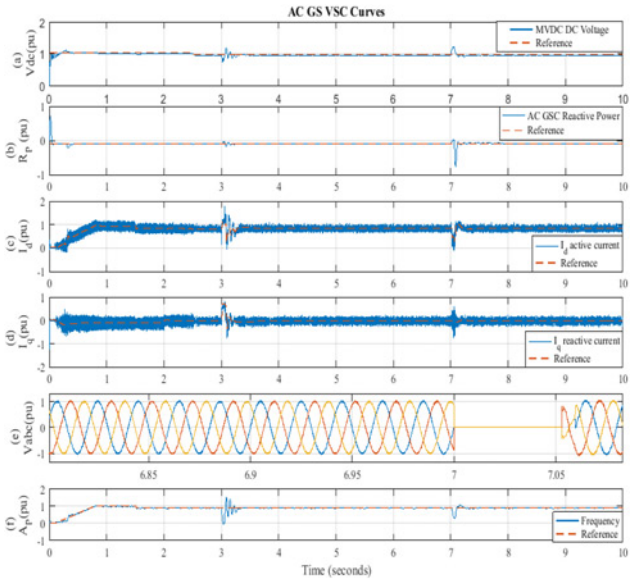

Fig. 6 *AC grid side VSC curves for three-phase fault*

farm VSC side, the fault results in some oscillations in the active power as shown in Fig. 5*a* and a fall in the MVDC voltage as shown in Fig. 6*a*. Despite the effect of the fault, the active current control signals accurately track their corresponding reference values as observed in Figs. 5*c* and 6*c*. This regulates the MVDC voltage as well as the active power flow and balance between the varying DFIG wind farm power and the MVDC bus. The DC motor supply remains as in steady state condition unaffected by the fault.

When the fault is imposed on the AC grid VSC, there are no observable changes on the active power on the wind farm as it is too low and compensated by the AC grid side. However, the active power at the AC grid side VSC falls accompanied with some oscillations as seen in Fig. 6*f*. As expected, these tendency results in an instantaneous increase in MVDC voltage on the bus. The supply to the DC load through the DC/DC converter remains undisturbed. The active current control signals highly regulate the DC voltage by accurately tracking the reference signal despite the oscillations caused.

During the fault, the AC voltages on both sides are highly distorted as shown in Figs. 5*e* and 6*e*. Consequently, more reactive power is absorbed on the wind farm side VSC and AC grid VSC sides as shown in Figs. 5*b* and 6*b*, respectively. The reactive current controls signals accurately follow the reference values despite the fault with minimum deviations as in Figs. 5*d* and 6*d*.

When the fault is incident on either sides of the MVDC system, the MVDC voltage rises while the active power flow falls in each of the cases reversing the power from the fault point to reduce its severity. In spite of these effects, the supply to the DC load through the DC/DC converter remains largely unaffected. The reactive power flow is independently and highly controlled on the wind farm VSC and AC grid VSC for AC voltage support on either side. When the fault is cleared, the oscillations caused in the DC voltage, active and reactive power decay quickly and normal operation resumes.

4 Conclusion

The mathematical modelling, simulation and analysis of a VSC MVDC network with DFIG wind farm integrated under constant active power control (wind farm side) and constant DC voltage control (AC grid side) in variable wind speed conditions have been studied. In steady-state, the DC voltage and active power flow and balance are highly controlled. The supply voltage to the DC load through the DC/DC converter remains constant. The MVDC network acts as a reservoir that absorbs the variable DFIG wind power and transforms it to a stable supply system. During the three-phase AC fault on the wind farm VSC and AC grid side VSC, the DC voltage and active power increase slightly. However, the supply to the DC load through the DC/DC converter remains undisturbed. The control signals accurately follow the reference values during three-phase fault and normal network operation resumes when the fault is cleared. Therefore, the MVDC network is stable with fast dynamic response.

5 References

[1] Reed G.F., Grainger B.M., Sparacino A.R., *ET AL.*: 'Ship to grid: Medium-voltage DC concepts in theory and practice', *IEEE Power Energy Mag.*, 2012, **10**, (6), pp. 70–79
[2] Bathurst G., Hwang G., Tejwani L.: 'MVDC – the new technology for distribution networks'. 11th IET Int. Conf. AC and DC Power Transmission, Birmingham, UK, 2015, pp. 1–5
[3] Bosich D., Vicenzutti A., Pelaschiar R., *ET AL.*: 'Toward the future: the MVDC large ship research program'. 2015 AEIT Int. Annual Conf., AEIT 2015, Naples, Italy, 2016
[4] Reed G.F., Grainger B.M., Sparacino A.R., *ET AL.*: 'Medium voltage DC technology developments, applications, and trends'. CIGRE US National Committee 2012 Grid of the Future Symp., Kansas City, MO, U.S.A., 2012, pp. 1–6
[5] Sparacino A.R., Grainger B.M., Kerestes R.J., *ET AL.*: 'Design and simulation of a DC electric vehicle charging station connected to a MVDC infrastructure'. 2012 IEEE Energy Conversion Congress and Exposition (ECCE), Raleigh NC, 2012, pp. 1168–1175
[6] Mura F., De Doncker R.W.: 'Design aspects of a medium-voltage direct current (MVDC) grid for a university campus'. 8th Int. Conf. Power Electron. – ECCE Asia 'Green World with Power Electron. ICPE 2011-ECCE Asia, Jeju, South Korea, 2011, pp. 2359–2366
[7] Korompili A., Sadu A., Ponci F., *ET AL.*: 'Flexible electric networks of the future: project on control and automation in MVDC grids'. Int. ETG Congress 2015, Bonn, Germany, 17–18 November 2015, pp. 556–563
[8] Yang M., Xie D., Zhu H., *ET AL.*: 'Architectures and control for multi-terminal DC (MTDC) distribution network ü a review'. 11th IET Int. Conf. AC and DC Power Transmission, Birmingham, UK, 2011, pp. 1–7
[9] Slootweg J.G., Polinder H., Kling W.L.: 'Dynamic modelling of a wind turbine with doubly fed induction generator'. 2001 Power Engineering Society Summer Meeting, Vancouver BC, Canada, 2001, pp. 644–649
[10] Edrah M., Lo K.L., Anaya-lara O., *ET AL.*: 'Impact of DFIG based offshore wind farms connected through VSC-HVDC link on power system stability'. 11th IET Int. Conf. AC and DC Power Transmission, Birmingham, UK, pp. 1–7
[11] Taylor E., Korytowski M., Reed G.: 'Voltage transient propagation in AC and DC datacenter distribution architectures'. in 2012 IEEE Energy Conversion Congress and Exposition, ECCE 2012, Raleigh, NC, USA, 2012, pp. 1998–2004
[12] Nguyen T., Yoo H.J., Kim H.M.: 'A comparison study of MVDC and MVAC for deployment of distributed wind generations'. IEEE Conf. on Sustainable Energy Technologies (ICSET), Hanoi, Vietnam, 2016, pp. 138–141
[13] Saeedifard M., Graovac M., Dias R.F., *ET AL.*: 'DC power systems: challenges and opportunities'. Power and Energy Society General Meeting 2010 IEEE, Providence, RI, USA, 2010, pp. 1–7
[14] Rahman H., Xu L.: 'Protection of large partitioned MTDC networks using DC–DC converters and circuit breakers', *Prot. Control Mod. Power Syst.*, 2016, **1**, (19), pp. 1–9
[15] Sarrias-mena R., Fernández-ramírez L.M., García-vázquez C.A., *ET AL.*: 'Modelling and control of a medium-voltage DC distribution system with energy storage'. 2016 IEEE Int. Energy Conf. (ENERGYCON), Leuven, Belgium, 2016, pp. 1–6
[16] Qu L., Qiao W.: 'Constant power control of DFIG wind turbines with supercapacitor energy storage', *IEEE Trans. Ind. Appl.*, 2011, **47**, (1), pp. 359–367
[17] Haileselassie T.M.: 'Control, dynamics and operation of multi-terminal VSC-HVDC transmission systems' (PhD Thesis, Department of Electric Power Engineering, Norwegian University of Science and Technology, Trondheim, Norway, 2012)
[18] Qiao W., Venayagamoorthy G.K., Member S., *ET AL.*: 'Real-time implementation of a STATCOM on a wind farm equipped with doubly fed induction generators', *IEEE Trans. Ind. Appl.*, 2009, **45**, (1), pp. 98–107
[19] Pinares G., Bongiorno M.: 'Modeling and analysis of VSC-based HVDC systems for DC network stability studies', *IEEE Trans. Power Deliv.*, 2016, **31**, (2), pp. 848–856
[20] Imhof M., Member S.: 'Dynamic modeling of a VSC-HVDC converter'. Power Engineering Conf. (UPEC), 2013 48th Int. Universities, Dublin, Ireland, 2013, pp. 1–6
[21] Belmans R., Cole S., Beerten J.: 'Generalised dynamic VSC MTDC model for power system stability studies', *IEEE Trans. Power Syst.*, 2010, **25**, (3), pp. 1655–1662

6 Appendix 1

DFIG wind farm

Capacity = 21 MW
Nominal wind speed: 11 m/s
GSC current regulator: K_p (1.4); K_i (9)
RSC current regulator: K_p (1.2); K_i (12)

AC grid/DFIG wind farm VSC side

Voltage = 35 kV
Inductance = 8.2×10^{-3} H
Transformer: 20 MVA; 35/10 kV, 0.15 pu
AC filter (high pass): 2.0 MVAr, 15(Q)
AC reactor: 0.15 pu
DC capacitor = 4000 μF
DC filter: 0.5 Ω; 60×10^{-3} H; 30×10^{-5} F
DC reactor: 0.031 Ω; 5×10^{-3} H

DC cable

5 km length; 2 pi sections; 1.39×10^{-2} Ω/km;
1.59×10^{-4} H/km; 2.31×10^{-7} F/km

DC motor load

220 kW, 700 V, 1750 rpm and field excitation 500 V

DC/DC converter

Switching frequency = 2000 Hz
Input filter: 0.01 F, 0.1472 Ω
Output filter: 10 Ω, 10×10^{-3} H; 0.1474 Ω, 0.01 F

Tuned controller gains

Current controller: $K_p = 24.1$; $K_{i/s} = 8.5$
Voltage controller: $K_p = 1.0$; $K_{i/s} = 42.0$
Active power controller: $K_{i/s} = 20.0$
Reactive power controller: $K_{i/s} = 20.0$